Journal of Energy and Power Engineering 7 (2013) 2321-2335

Assessing Micro-generation's and Non-linear Loads' Impact in the Power Quality of Low Voltage Distribution Networks

Paulo Bonifácio[1], Susana Viana[2], Luís Rodrigues[1] and Ana Estanqueiro[1]

1. Energy Analysis and Networks Unit, Portuguese National Laboratory of Energy and Geology, Lisbon 1649-038, Portugal

2. Solar Energy Unit, Portuguese National Laboratory of Energy and Geology, Lisbon 1649-038, Portugal

Received: December 27, 2012 / Accepted: April 01, 2013 / Published: December 31, 2013.

Abstract: Distribution networks face an increasing penetration of solar PV (photovoltaic) and small WTG (wind turbine generator) as well as other forms of micro-generation. To this scenario, one must add the dissemination of non-linear loads such as EV (electric vehicles). There is something in common between those loads and sources: the extensive use of power electronic converters with commutated switches. These devices may be a source of medium-to-high frequency harmonic distortion and their impact on the local distribution grid must be carefully assessed in order to evaluate their negative impacts on the network, on the existing conventional loads and also on other active devices. In this paper, methodologies to characterize effects such as: harmonics, network unbalances, damaging power line resonance conditions, and over/under voltages are described and applied to a real local grid configuration.

Key words: Micro-generation, distribution network, power quality, harmonics, smart grid, electric vehicle.

1. Introduction

DG (distributed generation) is an ever growing reality. As energy prices tend to rise, so does the consumer's attraction for installing some type of renewable MG (micro-generation) in his household. For example, the Portuguese MG capacity was 81 MW by the end of 2012, of which 99% were solar PV (photovoltaic) systems. To this, one must add the advent of large scale integration of grid connected EV (electric vehicles) both in the common charging operation G2V (grid-to-vehicle) and the less deployed V2G (vehicle-to-grid) mode. This new scenario of large penetration of renewable DG and EV type loads presents a challenge to distribution grid operators: the degradation of local power quality.

Corresponding author: Ana Estanqueiro, Ph.D., research fields: grid integration of wind power, power systems with high wind penetration, micro-generation, power quality and planning methodologies for wind deployment. E-mail: ana.estanqueiro@lneg.pt.

One of the power quality issues to address is the harmonic content since active systems produce undesirable effects in the equipment connected to the electrical grid [1-4]. Such effects may be divided into resonance, transient and steady-state disturbances. Resonance concerns the amplification of harmonic currents for frequencies in the vicinity of the system resonance frequency, due to the existence of capacitor banks for reactive compensation, which can fail in these situations due to over current problems. Fast transient effects are related to switching occurrences in grid control equipment. The harmonic disturbances occurring in the grid's steady state operation are normally due to active loads (and sources) and can produce vibrations and acoustic noise in transformers, reactors and rotating machines.

Renewable MG units are essentially connected to the electrical DN (distribution network) and act as harmonic sources during their whole range of operation

[5]. EV chargers in both modes of operation, G2V and V2G, contribute to local grid power quality degradation, by emitting harmonics. Although concerns related to the impact of large scale integration of DG and EV have been addressed by some authors [6-8], little work was done and reported about the evaluation of the impact of these new loads and sources in terms of harmonic propagation in low voltage DN, an issue that is addressed by this paper. That concern is reinforced by the high expectations on the large scale deployment of electric mobility. To achieve that objective, short-term flexibility of EV's use is essential; this flexibility brings the necessity of quick charging stations (30 min approx.) which leads to several technical questions regarding the integration of high power charging stations in urban, rural and/or remote weak grid areas, as noted by Bingchang et al. [9], where local demand, short term active power supply and reactive power compensation are studied, active filters, and control methodologies are proposed as means to solve the harmonics problem.

As for power quality in MG, in Ref. [10], an impedance-based approach to detect and characterize renewable energy system harmonic resonance is developed to evaluate harmonic resonance behaviour with single and three-phase grid parallel inverters. In the PV generation case, cloud-induced transients in the output power are a barrier when its penetration reaches higher levels in DG systems. Such transients may cause voltage flicker or excessive operation of the distribution grid voltage regulating equipment. The impact of high PV penetration is discussed by Ari and Baghzouz [11] and the results indicate that voltage flicker is not a large concern in the PV case, but the transformers tap changers operate excessively, leading to premature ageing of these equipment.

A review of the state of the art and of the ambitions and goals of both EV and MG sectors reveals the need to develop planning DN tools capable of evaluating all those different issues in a single simulation tool, as the one presented in this work. This paper presents a methodology developed to assess the situations described above, i.e., the impact of DG equipped with power converters, non-linear and common household loads on harmonic distortion. The work began with REIVE project [12, 13], whose main purpose was to assess the impact of EVs in the LV (low voltage) distribution network.

In Section 2, the simulation models, the SDA concept and the low voltage distribution grid configuration are presented. In Section 3, the cases considered for the simulations are described and their results are shown. In this section, there is also a brief comparison between real PV inverter current signals and the theoretical ones initially used in the simulations. Conclusions of the work are drawn and recommendations are given in Section 4.

2. Simulation Models

The basis of the developed methodology to assess the relevant aspects associated with the power quality of distribution networks is a LV/MV 3 phase balanced/unbalanced power line simulator. At the core of this tool an entity was created, the SDA (smart domestic agent). The SDA is a multi-configurable power consumer/producer component.

This agent is used as the base building block of the low voltage power distribution network and integrates models for different power producer/consumer devices that can be commonly encountered in the distribution network. Those models have a high degree of configurability which allows the user to swiftly change the characteristics of the connected components, testing different case studies for the same core network without the need to perform a deep manual reconfiguration of the line or the models themselves.

2.1 Smart Domestic Agent

The SDA agent supports the usual consumer loads and other models that allow the simulation of multiple types of loads and/or power generation, i.e., PV generation, micro wind turbines, nonlinear loads and

energy storage units. Multiple types of SDA can be presented at any given time in the simulation without impairing on others.

Each SDA possesses two types of model: a physical model and a current injection/consumption model. The physical model is more resource intensive, but allows the assessment of all the generator components and the determination of the line currents and bus voltages. This model enables the simulation and assessment of the variability of the renewable energy resource, i.e., by feeding solar irradiance (for PV) and wind speed time series (for micro wind turbines).

The current injection/consumption model follows the existing recommendations [14, 15] for micro-generation. The fundamental (i.e., 50 Hz) component currents and their relevant harmonics are modelled through ideal current sources and this is done to allow for the simulation of the interaction of the power electronics and non-linear load components of each SDA with the interface of the power grid. The harmonic current sources were connected in parallel with each other and with the source for the fundamental current value.

In Fig. 1, the block diagram of SDA is presented. This agent is built around four main components, a PV generator, a micro wind generator, a typical domestic load (i.e., P, Q load) and a battery charger load. The user can choose if all or just some of these components are present in any SDA, thus allowing the simulation to reflect a wide range of cases.

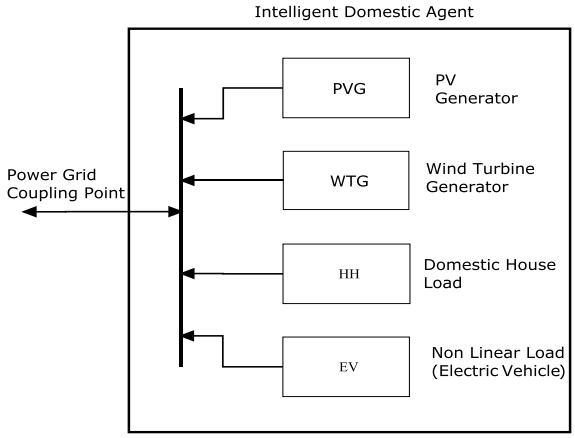

Fig. 1 Block diagram of the smart domestic agent.

2.2 Photovoltaic Generator

2.2.1 Physical Model

This model needs the input of meteorological data. The block diagram in Fig. 2 shows the proposed PVG (PV generator) model; it is composed by a subset of three different subsystems that interconnect with each other. A current-voltage, I (V), characteristic curve simulates the PV module response to solar irradiance; a MPPT (maximum power point tracker) enables optimum power production; finally an inverter provides interconnection to the AC grid. The I (V) curve block receives the ambient temperature (T_{amb}) and global irradiance (G_i) data, then uses this data to generate the PV module current (I_{PV}) that is then fed to the MPP tracker. The MPPT subsystem feeds optimum voltage (V_{dc}) and current (I_{dc}) data to the inverter block that outputs the current (I_o) to be injected to the electrical grid at the PCC (point of common coupling).

2.2.2 Current Model

The current model used for PV was the most complete of the ones available for this work. Three sources of current signals for PV inverters where available. A theoretical model developed for the REIVE project—Smart grids with electric vehicles, V2G and G2V [13]; and two harmonic current injection models with current signals obtained from the measurement of current signals in active working, grid-tied, solar inverters (<4 kW).

The current signals obtained from the solar inverter, devices (S) and (F) as those of the theoretical model (T), were converted to the frequency domain with FFT (fast Fourier transform). The harmonic spectra determined the value of each of the current harmonics for each signal, from where the most relevant harmonics to be modelled were selected (i.e., those whose power exceeded 1 W). Sample signals for (S), (F) and (T) devices are shown in Fig. 3.

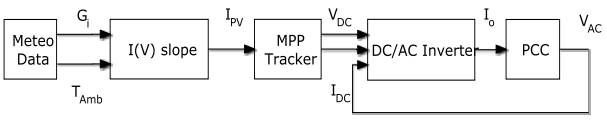

Fig. 2 PVG (photovoltaic generator) physical model.

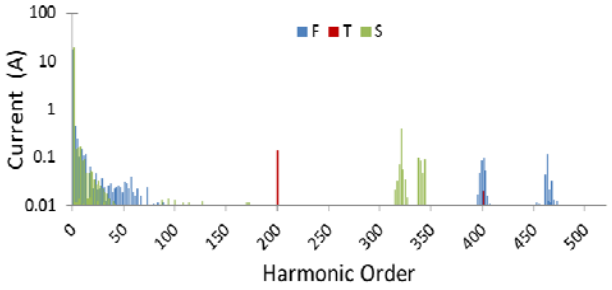

Fig. 3 Current harmonic spectra for (S), (F) and (T) inverter devices.

Analysing the sample signals in Fig. 3, it can be seen that there is some difference between both devices. The measured harmonic content for device (S) has the most harmonic current above the 10 kHz range, (0.2 A at 20 kHz). Device (F) has higher 3rd and 7th harmonics but lower 399th harmonic, 0.45 A, 0.25 A and 0.13 A for the 3rd, 7th and 399th harmonic, respectively.

2.3 Wind Turbine

2.3.1 Physical Model

The WTG (wind turbine generator) model is composed of 3 main subsystems as depicted in Fig. 4. The simulator starts by feeding wind speed data into the rotor/transmission subsystem; and from there the mechanical shaft speed (ω_{mec}) is passed to the generator/rectifier subsystem. The rectifier outputs DC voltage and current (V_{dc}, I_{dc}) that are fed to the inverter subsystem, which in turn outputs the current (I_o) to be injected into the grid at the PCC.

2.3.2 Current Model

The current model for the wind turbine was built in the same way as the current model applied to the PV generator; the currently used data for the wind turbine was obtained from a simulator developed for the REIVE project.

2.4 Battery Charger

2.4.1 Physical Model

The proposed battery charger model is built around a low power charge mode. This model corresponds to a typical vehicle on-board charger. The charger operates with a charging rate from 0.1 *C* to 0.2 *C* of the battery

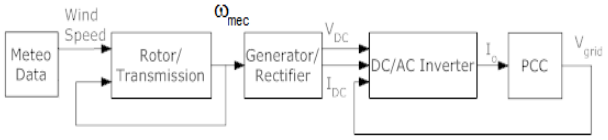

Fig. 4 Micro WTG (wind turbine generator) physical model.

pack power capacity (*C*), i.e., for a 25 kWh battery the charger supplies 3 kW to 4 kW to the battery pack [16, 17].

The model is composed of three main components; a rectifier connected to a PCC, a DC/DC power converter and charge controller which controls the battery charge and the battery pack itself, the proposed model is represented in Fig. 5. The AC/DC rectifier takes the voltage (V_{ac}) from a PCC in the power grid, it then calculates the direct current value (I_{dc}) and transfers it to the charge controller subsystem; using the voltage and current data from the battery pack, the charge controller generates a charging current (I_{Ch}) which feeds the battery pack.

2.4.2 Equivalent Model

The battery charger equivalent model was built following the recommendations of Ref. [17] and is based in a parallel *RL* load connected in series with a harmonic current source model, as show in Fig. 6. The *R* load represents the battery's active power consumption at fundamental frequency; *L* represents the reactive component brought by the charger in partial charge conditions; finally, the charger power electronic components are represented by the current sources.

2.5 House Consumer Model

The proposed model for house consumption is composed of a series *RL* load; the *R* value representing the power consumption component (mainly resistive) of the devices connected in the house such as lighting and heating. The *L* value represents the reactive component of the load and is used to model loads such as electric motors that are part of some domestic appliances like blenders or washing machines.

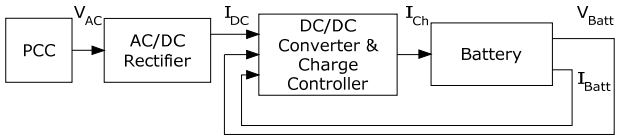

Fig. 5 Battery charger physical model (EV).

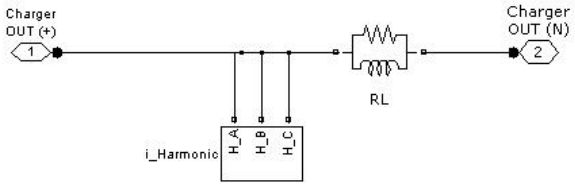

Fig. 6 Electric vehicle charger linear model.

2.6 Distribution Network Model

The base distribution network used for this work was adapted from a real low voltage three phase unbalanced distribution network (400 V_{ac}) where single (230 V_{ac}) and three phase users are connected [18]. This network, shown in Fig. 7, is composed of six branches connected to the secondary of a medium to low voltage PT (power transformer). In each of the branches single and three phase users are unevenly connected. In the distribution network diagram, three phase loads are represented by (///) with the number ($A\times$) corresponding to the quantity of connected users. In the same way, single phase users are represented by (//). The doted circle numbers correspond to the bus number and the [B] number indicates the connection of the line branch to the PT.

Single phase users are considered as common domestic consumers and are represented by a single SDA connected per phase and per bus; three phase users are considered as small business or single large domestic users and are represented by a three phase load with active and reactive components only (i.e., no current harmonics injection were considered).

For simulation purposes, consumers connected to the same bus were aggregated as a single SDA per phase. This simplification procedure applied to a bus with 9 consumers would lead to 1 SDA per phase (3 in total), each one with the equivalent load for 3 consumers. When the number of consumers did not allow for an even load distribution per SDA (4, 5, 7…),

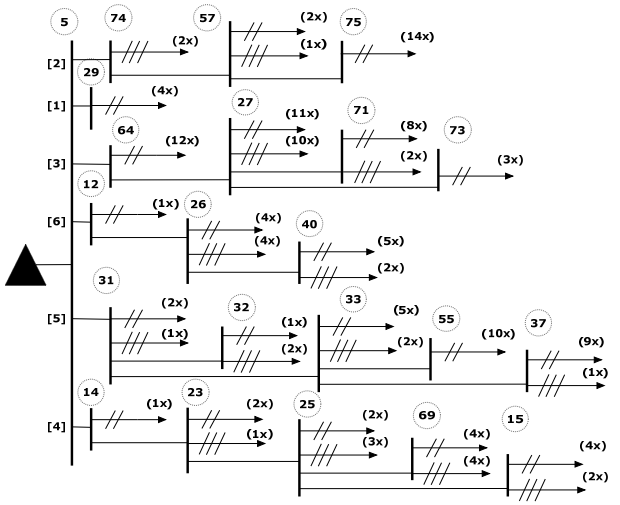

Fig. 7 Distribution network layout.

the total load value was divided by the number of consumers, with each SDA receiving an uneven part of this load base value. For a 4 SDA distribution this would correspond to a (2, 1, 1) configuration, meaning that two consumers are connected to the first phase, and one consumer is connected to each one of the other two phases.

As no data was available regarding the neutral line structure, it was considered that all the clients neutral connections where made to a single common connection point at the PT.

This proposed method allowed for the simulation of a heavily populated distribution network as the model used was composed of more than 140 consumers.

2.7 Configuration and Simulation

Initial network layout and object placement (SDA), are done manually in the Simulink GUI (graphic user interface). After that all new configurations (including line parameters) can be done via script; this option was chosen to allow for a quicker model reconfiguration. Fig. 8 shows the detail of the layout for the 2nd branch of the modelled DN.

After the simulation is completed the results can be seen in the sampled points of interest. Then the model can be quickly reconfigured for the test of new scenarios. Fig. 9 shows the functional block diagram for simulation operation.

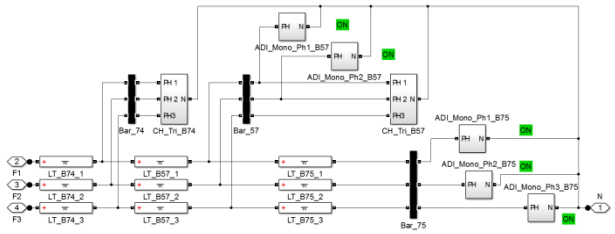

Fig. 8 Detail of the implemented model for branch 2.

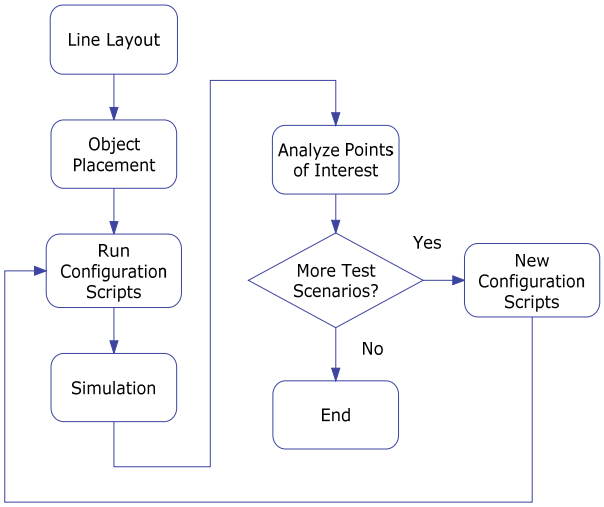

Fig. 9 Functional block diagram for simulation.

3. Case Studies and Results

3.1 Modelled Case Studies

In order to assess the power quality and harmonic distortion of the DN voltages and currents, four case study scenarios were considered, they are described in Table 1.

Case I has a peak load scenario and can only be used as reference. Cases II to IV present a load scenario of 25% of the peak load, enabling the visualisation of the impact of micro-generation and EV penetration in the power quality of the local grid.

3.1.1 Case I—Full Peak Load—SDAs with Loads Only

The first case scenario reflected the technical characteristics of the distribution grid. Peak load power consumption by SDA in each grid branch is presented in the Appendix.

3.1.2 Case II—25% of Peak Load—SDAs with Non-linear Loads

For the second case scenario, only 25% of the peak load value was considered and all the connected SDAs were enabled with non-linear loads corresponding to EVs.

Table 1 Test scenarios.

Case	Conditions
I	Loads only—full peak load
II	Loads—25% full peak load EV—present in all SDA.
III	Loads—25% full peak load EV—present in all SDA. Micro-generation—present in all SDA.
IV	Loads—25% full peak load EV—1 per bus Micro-generation—present in all SDA.

3.1.3 Case III—25% of Peak Load—SDAs with Heavy Penetration of Non-linear Loads and Micro-generation

The third case scenario is built on top of the second case; the non-linear loads are complemented with the introduction of some type of micro-generation. A PVG or WTG was placed in the SDAs of each bus. This approach allowed for the evaluation of the impact of the introduction of micro-generation in the phase current and voltage unbalance. The impact on the voltage and current distortion caused by the introduction of micro-generation sources and heavy penetration of EVs could also be evaluated.

3.1.4 Case IV—25% of Peak Load—SDAs with Some Non-linear Loads and Heavy Penetration of Micro-generation

The final test scenario considered the conditions of the Case III and added more micro-generation. EV penetration was reduced to 1 EV per bus in order to lower their impact in the simulation. This option was chosen in order to assess if the presence of micro-generation power sources could help in the voltage dip prevention and in the grid stabilization capability.

3.2 Results

Values for the voltage and its THDv (total harmonic distortion) in the low voltage secondary side of the power transformer are presented for all considered

cases. To perform the current analysis and calculate its total harmonic distortion (THDi), measurements were taken at the branches 1 to 6 in the low voltage side of the power transformer. The branch identification is as follows:

Branch 1—between bus 5 and bus 29;
Branch 2—between bus 5 and bus 75;
Branch 3—between bus 5 and bus 71;
Branch 4—between bus 5 and bus 15;
Branch 5—between bus 5 and bus 55;
Branch 6—between bus 5 and bus 40.

Voltage values in the bus were all branches are connected (bus 5) and in the most distant buses of each branch were taken. The identification of the lines connected to these buses is as follows:

Line 0—from the secondary of the PT to bus 5;
Line 1—from bus 5 to bus 29;
Line 2—from bus 57 to bus 75;
Line 3—from bus 27 to bus 71;
Line 4—from bus 25 to bus 15;
Line 5—from bus 33 to bus 55;
Line 6—from bus 26 to bus 40;
Line 7—from bus 64 to bus 27;
Line 8—from bus 25 to bus 69.

Lines 7 and 8 are not connected to the most distant buses from the PT, but were included because their analysis is of interest, for they are the most heavily loaded buses in the low voltage DN.

For Cases III and IV the used current signals (T) were augmented with signals obtained from two different grid-tied solar inverters, devices (S) and (F), both in the 4 kW power range. For analysis purposes data is shown in detail for the selected lines and buses.

3.2.1 Voltages at the Secondary Side of the Power Transformer and Currents in Line 0

In Fig. 10, it can be observed that in Cases I to III the voltages at the secondary of the PT oscillates between 0.991 p.u. and 0.996 p.u. (per unit) in all three phases. In Case IV, the voltage is very close to 1 p.u. varying from 0.998 p.u. to 0.999 p.u., except for phase 2 where the voltage is close to 0.994 p.u.. Regarding the THDv,

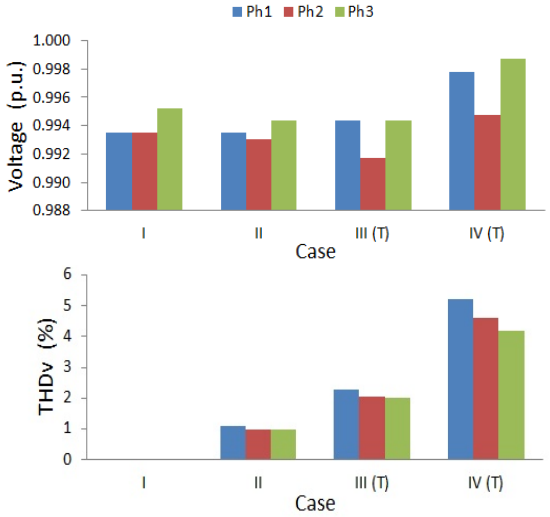

Fig. 10 Voltage and voltage distortion (THDv) at bus 5.

as the penetration of micro-generation and EVs is increased, so does the distortion, as seen in the Cases I to III. In Case IV, the reduction of loads from EV sources more than doubles the voltage distortion seen across all the three phases.

Fig. 11 shows the values and distortion of the current for the three line phases. Some current unbalance can be seen in Cases I and II. With the introduction of micro-generation the nature of the unbalance changes, as more current flows in phases 2 and 3 when compared to phase 1 and as opposed to what is seen in the first two cases. The most noticeable effect occurs in the neutral current as values spike up in Cases III and IV; in Case IV, with the addition of micro-generation, it can be seen that the value of neutral current is of the same magnitude of the current flowing in phases 1 to 3.

Regarding the current distortion; it increases with the addition of EV and micro-generation in Cases I to III. In Case IV, the reduction of EVs also leads to an increase of THDi, this situation seems to indicate some level of damping on the distortion due to the non-linear load of the EV.

Fig. 12 represents typical signals obtained from the simulation in the low voltage side of the PT.

Tables 2 and 3 present the simulation results for the voltage at bus 5 and current at Line 0 of the distribution network.

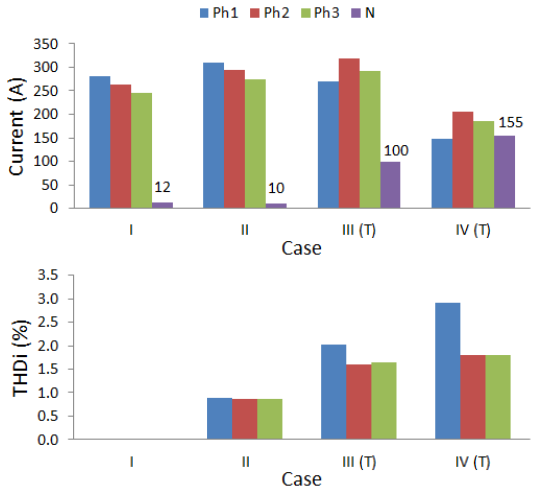

Fig. 11 Current and current distortion (THDi) per phase and in the neutral measured at Line 0 (note that the neutral current distortion is not presented).

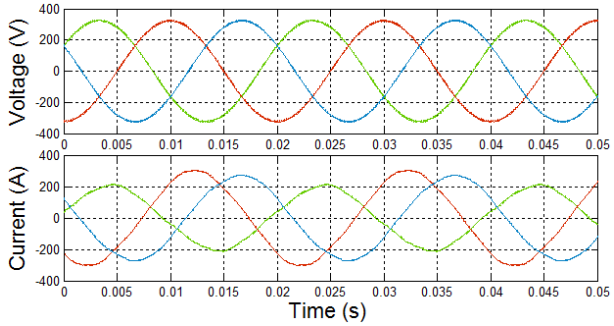

Fig. 12 Voltages at the low voltage side of the PT and currents in Line 0, for Case IV (T).

Table 2 Voltage and THD_v at low voltage side of the PT.

Case	Bus 5					
	Ph1		Ph2		Ph3	
Voltage	V (p.u.)	THD_v (%)	V (p.u.)	THD_v (%)	V (p.u.)	THD_v (%)
I	0.993	0.00	0.993	0.00	0.995	0.00
II	0.993	1.09	0.993	0.99	0.994	0.96
III (T)	0.994	2.28	0.992	2.06	0.994	2.00
III (S)	0.994	1.75	0.992	1.58	0.995	1.54
III (F)	0.994	1.51	0.992	1.38	0.995	1.32
IV (T)	0.998	5.23	0.995	4.62	0.999	4.19
IV (S)	0.998	1.62	0.994	1.41	0.999	1.26
IV (F)	0.998	1.26	0.994	1.06	0.999	0.92

Analysis of the data presented in these tables indicates that the introduction of micro-generation is useful at uplifting the voltage at the secondary of the PT. It is also noteworthy that the association of micro-generation with EVs reduced the current measured in most of the line branches.

Table 3 Current and THD_i at line 0.

Case	Line 0							
	Ph1		Ph2		Ph3		N	
Current	I (A)	THD_i (%)	I (A)	THD_i (%)	I (A)	THD_i (%)	I (A)	
I	281.50	0.00	262.90	0.00	245.80	0.00	11.51	
II	309.30	0.88	295.10	0.87	274.60	0.86	10.34	
III (T)	270.90	2.02	318.10	1.61	291.70	1.65	99.89	
III (S)	264.50	1.78	321.70	1.37	295.40	1.38	118.80	
III (F)	266.80	2.88	320.60	2.25	294.60	2.26	112.60	
IV (T)	147.70	2.91	204.90	1.81	184.90	1.81	154.50	
IV (S)	141.10	2.63	213.80	1.50	194.30	1.49	184.00	
IV (F)	143.30	4.63	210.70	2.81	191.10	2.81	174.10	

In Cases III and IV, the association referred above reduced the measured current distortion (THD_i), but on the downside, increased the voltage distortion (THD_v) that has a smaller fluctuation window (max. 8%).

Neutral currents due to phase imbalance become noticeable with the introduction of EV type loads, although without significant effect (Case II). The introduction in Cases III/IV of a heavy penetration scenario of micro-generation gives rise to a significant increase of neutral current.

For Case IV, the damping effect performed by the EV type loads can be noted. If those loads are limited, a significant increase on measured voltage distortion for all of the line phases is seen. The same type of distortion also shows for current, albeit with a lower value and focused on a single phase. The neutral current rises even more than in the previous case and reaches the same order of magnitude of the currents flowing in all the three line phases.

3.2.2 Measured vs. Theoretical Signals

For Cases III and IV, the simulation was performed with all the available PV current signals, (T), (S) and (F). Figs. 13 and 14 show a comparison of those signals at the LV side of the PT, bus 5, for Case III.

Comparing the results obtained with the measured current signals in Tables 2 and 3, for Case III/(S)/(F) and Case IV/(S)/(F), it can be noted that the harmonic current content of the power electronics devices that build-up the solar power inverters have a significant impact in the voltage and current distortion measured

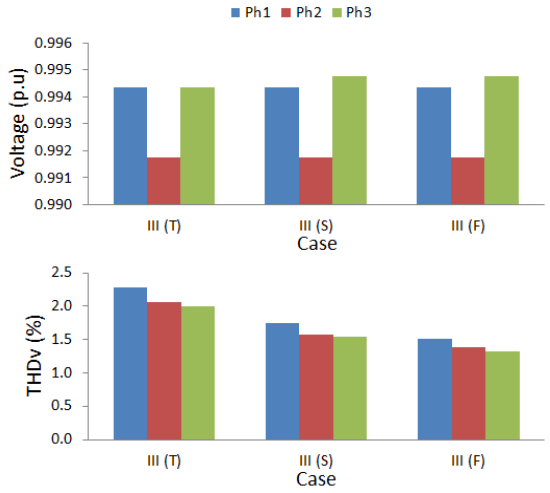

Fig. 13 Voltage amplitude and distortion for all three sampled signals in Case III—bus 5.

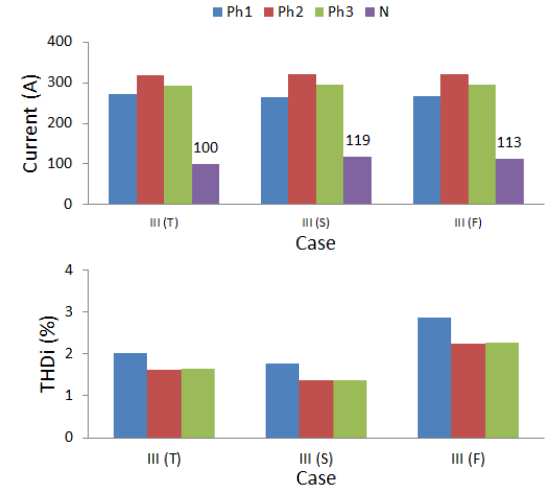

Fig. 14 Current amplitude and distortion for all three sampled signals in Case III—Line 0.

in the bus/line. In Cases IV (S) and IV (F), the later THD_i is higher than the former; 4.63% versus 2.63%, for phase 1. As for the THD_v the situation is the reverse, as IV (S) has a greater measured distortion than IV (F); 1.26% versus 1.62%.

These results can be largely explained by the line impedance diagram, Fig. 15, and the lines distance to the PT. As lower frequency harmonic currents face lower equivalent impedance, they tend to propagate through the network. On the other hand, higher frequency harmonic currents face higher impedance, tending to be transduced into voltage harmonics and to propagate less throughout the DN. As impedances are distributed along the length of the lines, the line

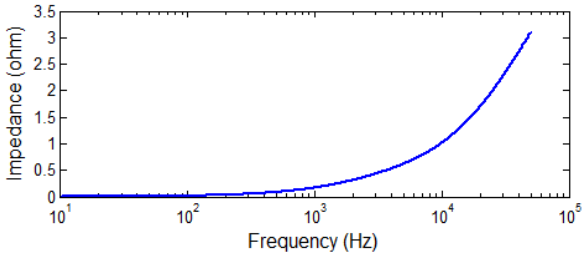

Fig. 15 Distribution network line impedance for phase 1.

distance to the transformer also plays a role in the harmonic propagation in the network. The longest distance to the PT occurs in bus 71 (Line 3) whose connection is placed at 463 m from the PT. This distance does not allow for the complete dissipation of the low power harmonics; additionally, for frequencies higher than 10 kHz, line impedance rises above 1 ohm reinforcing the impact of high frequency current harmonics in voltage distortion.

3.2.3 Branch 3: Voltages at Bus 27 and 71; Currents in Lines 7 and 3

Branch 3 is one of the heaviest loaded branches of the distribution network. Results are show for the longest lines and the heaviest loaded buses. At the far most location from the PT, bus 71, micro-generation helps to lift the voltage level leading to values above 0.90 p.u. for each of the 3 phases, as can be seen in Fig. 16. There is a trade-off however, the THD_v has a slight increase, although its value is still under current normative values for voltage distortion (EN 51160 and IEC 61000-2-2 Standards) [19, 20].

Fig. 17 shows the current through Line 3. A slight current unbalance can be seen, and it becomes more significant with the limitation of EVs (Case IV). Looking at the most loaded bus of branch 3; bus 27, Line 7, in Fig. 18; the ability of micro-generation to assist, lifting lower voltage levels becomes evident.

In Fig. 18, the introduction of micro-generation enhances the average voltage but adds some THD_v. Voltage values are constantly above 0.93 p.u. for Case IV and close to 0.90 p.u. in Case III. As for the current, Fig. 19, the uneven distribution of loads and micro-generation becomes apparent for Case IV with a significant current unbalance for phase 2 relatively to

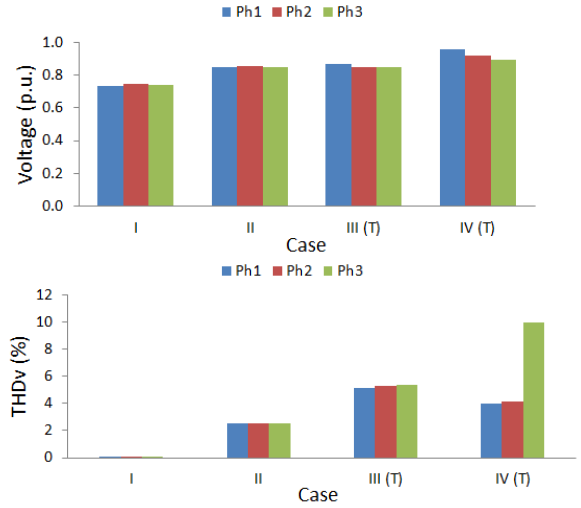

Fig. 16 (a) Voltage amplitude and (b) THD_v at bus 71 of branch 3.

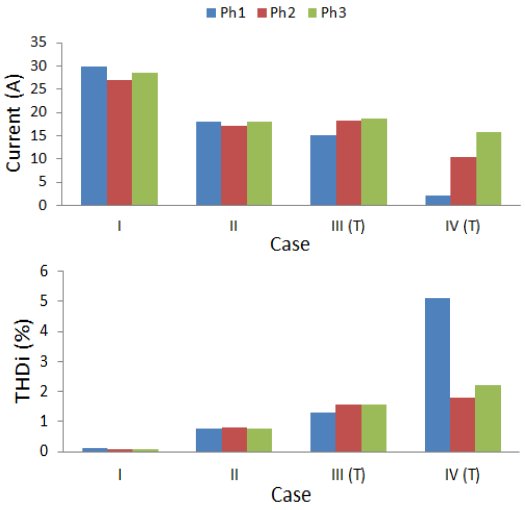

Fig. 17 Current amplitude and THD_i in Line 3 of branch 3.

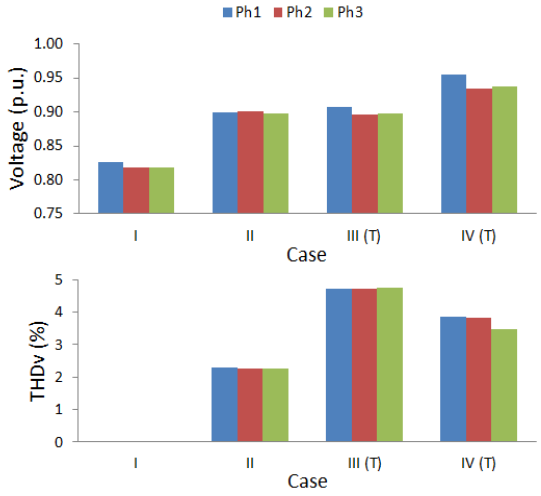

Fig. 18 Voltage amplitude and THD_v at bus 27 of branch 3.

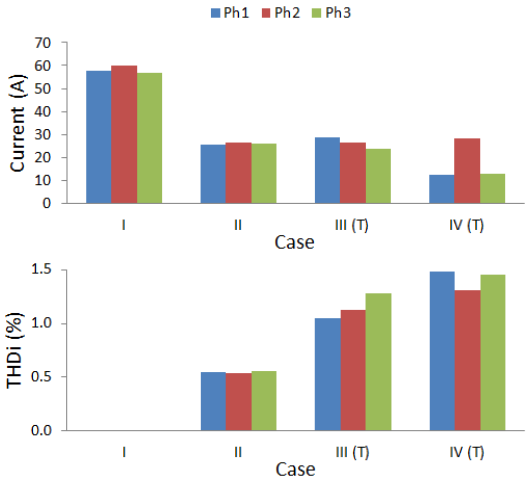

Fig. 19 Current amplitude and THD_i in Line 7 of branch 3.

phases 1 and 3. All these unbalances dispersed throughout the distribution network account for the neutral current values that are shown in Table 3.

3.3 Current and Voltage Distortion Limits According to Normative Standards

Normative standards for total harmonic distortion of current (THD_i) values are specified by IEC 61000-3-2 and are defined by equipment class. The maximum allowed current distortion supplied by the distribution network cannot exceed 15% [3, 21]. At this time, there is no specified normative that stipulates the maximum value of current distortion injected into the grid. This distortion value is calculated with harmonic values up to the 40th harmonic, i.e., 2,000 Hz.

For the voltage, total harmonic distortion values (THD_v) are specified by standard IEC 61000-2-2. The THD_v is calculated with harmonic values up to the 50th harmonic and must not exceed 8% [20].

Figs. 20 and 21 show the same voltage signal; bus 5, phase 1; with and without normative constrains.

When only the normative harmonic values are considered, THD values are always according to normative constrains. When the measurements range is expanded, there is a noticeable increase in measured distortion, both in voltage and current. Line resonance values which varied from 14 kHz to 17 kHz where extracted from Ref. [22]. Also, measured harmonic

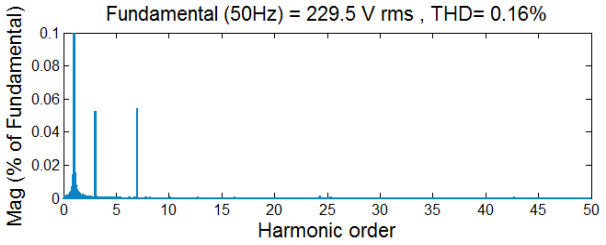

Fig. 20 Voltage distortion with normative values, at bus 5, phase 1, for Case IV (T).

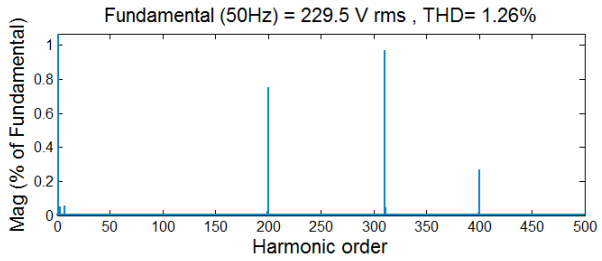

Fig. 21 Voltage distortion with total injected harmonic spectrum, at bus 5, phase 1 for Case IV (T).

values for devices (S) and (F) varied not only in current values but also in frequency according to solar irradiance; with harmonics ranging from 300th to 470th (Fig. 3). This situation is characteristic of switching power components that vary their duty cycle according to load and available power.

Some of these harmonics can occur on top of the line resonance conditions and lead to damaging events in the distribution network.

4. Conclusions

This paper presented a methodology to assess the impact of distributed micro-generation and non-linear loads in the power quality (harmonic content) of low voltage local distribution network. This was achieved with the introduction of a simulation tool composed of physical and harmonic current models for all of the different network components. The current signals can be obtained from database signals or obtained from external simulation of physical modelling for each component.

The simulation results show that in the case of unbalanced 3 phase low voltage networks, caution must be taken when placing a representative number of micro-generation sources, as the source's connection may deteriorate the line balance.

Results presented for branch 3 indicate that future work should be made regarding the placement of power inverters, as their proximity can adversely affect the normal operation not only of the local power grid but also of adjacent devices. These occurs by the reinforcement of local damaging harmonic components, that may not reach the PT but are present in the vicinity of the emitting source and can induce resonance conditions on the power devices connected nearby.

Finally, simulation results suggest that a pre-normative recommendation should be developed in order to enlarge the number of harmonics taken into account when calculating THD values. As it has been shown, harmonic current and voltage can appear near or on top of line resonance frequency, with severe consequences for grid operation and most of the connected equipment. Also, it must be considered that the ever-increasing penetration of low quality medium sized switch-mode power supplies (<1 kW) in a domestic environment, can lead to a growth of situations of line distortion and unbalance.

Acknowledgments

The authors would like to acknowledge partial support under the FCOMP-01-0124-FEDER-016080 project and would also like to extend their appreciation to Eng. Maria João Martins from LNEG for her contribution in the inverter data acquisition that led to the signals used in the simulations.

References

[1] EMC (electromagnetic compatibility)—General Guide on Harmonics and Interharmonics Measurements and Instrumentation, for Power Supply Systems and Equipment Connected thereto, Part 4-7: Testing and Measurement Techniques, IEC 61000-4-7 ed2.0, 2008.

[2] EMC (electromagnetic compatibility)—Power Quality Measurement Methods, Part 4-30: Testing and Measurement Techniques, IEC 61000-4-30 ed2.0, 2008.

[3] EMC (electromagnetic compatibility)—Consol. with am 1 & 2, Part 3-2: Limits—Limits for Harmonic Current Emissions (equipment input current nt nt per phase), IEC 61000-3-2 ed3.2, 2009.

[4] EMC (electromagnetic compatibility)—Voltage Fluctuations and Flicker in Public Low-Voltage Supply Systems, for Equipment with Rated Current Pat A per Phase and not Subject to Conditional Connection, Part 3-3: Limits—Limitation of voltage changes, IEC 61000-3-3 ed2.0, 2008.

[5] IEEE Standard 929-2000, IEEE Recommended Practice for Utility Interface of PV (photovoltaic) Systems, 2000.

[6] R.J. Ferreira, L.M. Miranda, R.E. Araújo, J.A.P. Lopes, A new bi-directional charger for vehicle-to-grid integration, in: IEEE PES ISGT 2011 Europe, Manchester, 2011, pp. 1-8.

[7] J.A.P. Lopes, F.J. Soares, P.M.R. Almeida, Integration of electric vehicles in the electric power systems, The Proceedings of the IEEE 99 1 (2011) 168-183.

[8] R.J. Rei, F.J. Soares, P.M.R. Almeida, J.A.P. Lopes, Grid interactive charging control for plug-in electric vehicles, in: 13th International IEEE Conference on Intelligent Transportation Systems (ITSC 2010), Funchal, 2010, pp. 386-391.

[9] C. Bingchang, N. Broy, A. Sourkounis, Pollution of high power charging electric vehicles in urban distribution grids, in: Compatibility and Power Electronics (CPE), Tallinn, 2011, pp. 34-39.

[10] J. Sun, X. Chen, A study of renewable energy system harmonic resonance based on a DG test-bed, in: Applied Power Electronics Conference and Exposition (APEC), 26th Annual IEEE, Fort Worth, 2011, pp. 995-1002.

[11] G.K. Ari, Y. Baghzouz, Impact of high PV penetration on voltage regulation in electrical distribution systems, in: 2011 International Conference on Clean Electrical Power (ICCEP), Ischia, 2011, pp. 744-748.

[12] P. Bonifácio, S. Viana, M.J. Martins, A. Estanqueiro, Task 2—Development of Tools for the Technical Impact Analysis of Microgeneration and Electrical Vehicles Integration, Project REIVE, LNEG, Lisboa, 2012.

[13] Projecto REIVE [Online], http://www.lneg.pt/iedt/projectos/264/ (accessed May 2012).

[14] IEEE—Task Force on Harmonics Modeling and Simulation, Modeling and simulation of the propagation of harmonics in electric power networks part I: Concepts, models and simulation techniques, IEE Transactions on Power Delivery 11 (1) (1996) 452-465.

[15] IEEE—Task Force on Harmonics Modeling and Simulation, Modeling and simulation of the propagation of harmonics in electric power networks part II: Sample systems and examples, IEE Transactions on Power Delivery 11 (1) (1996) 466-474.

[16] T. Olivier, D.A. Louis, Experimental validation of a battery dynamic model for EV applications, World Electric Vehicle Journal 3 (2009) 1076-1096.

[17] A. Kuperman, U. Levy, J. Goren, A. Zafranski, A. Savernin, High power Li-ion battery charger for electric vehicle, in: Compatibility and Power Electronics, 7th International Conference-Workshop, Tallinn, June 1-3, 2011, pp. 342-347.

[18] P. Bonifácio, S. Viana, L. Rodrigues, A. Estanqueiro, Project REIVE—Task 3: Test and Optimization of Tools for Power Quality and Harmonic Distortion Analysis, LNEG, Lisboa, 2012.

[19] Voltage Characteristics of Electricity Supplied by Public Distribution Systems, EN 50160, 2006.

[20] EMC (electromagnetic compatibility)—Part 2-2: Environment—Compatibility Levels for Low-Frequency Conducted Disturbances and Signaling in Public Low-Voltage Power Supply Systems, IEC 61000-2-2 ed2.0, 2002.

[21] Requirements for the Connection of Micro-Generators in Parallel with Public Low-Voltage Distribution Networks, EN 50438 ed. 1, 2007.

[22] B.K. Lee, M. Ehsami, A simplified functional simulation model for three-phase voltage-source inverter using switching function concept, IEEE Transactions on Industrial Electronics 48 (2) (2001) 309-321.

Appendix A: Current and THD_i per Branch

Tables A1 to A4 present the measured current and THD_i in selected branches connected to the low voltage side of the power transformer.

Table A1 Current and THD_i at branch 3.

Case	Branch 3					
	Ph1		Ph2		Ph3	
Current	I (A)	THD_i (%)	I (A)	THD_i (%)	I (A)	THD_i (%)
I	90.87	0.00	90.51	0.00	88.14	0.00
II	75.94	0.76	76.84	0.76	79.10	0.76
III (T)	68.46	1.52	80.50	1.53	80.54	1.56
III (S)	70.50	1.29	81.75	1.23	81.94	1.34
III (F)	69.81	1.86	81.32	2.33	81.46	2.34
IV (T)	44.09	1.88	48.96	1.8	48.3	1.78
IV (S)	46.66	1.49	51.84	1.57	51.61	1.54
IV (F)	45.79	2.32	50.85	3.10	50.48	3.09

Table A2 Current and THD_i at branch 4.

Case	Branch 4					
	Ph1		Ph2		Ph3	
Current	I (A)	THD_i (%)	I (A)	THD_i (%)	I (A)	THD_i (%)
I	67.85	0.00	56.33	0.00	51.10	0.00
II	71.55	0.83	69.33	0.83	56.85	0.84
III (T)	64.64	1.93	75.47	1.47	61.24	1.51
III (S)	61.92	1.79	76.14	1.30	61.08	1.28
III (F)	62.83	3.08	75.91	2.11	61.14	1.93
IV (T)	36.06	2.66	53.11	1.76	38.84	1.59
IV (S)	33.25	2.70	54.13	1.47	39.61	1.30
IV (F)	34.19	4.96	53.78	2.57	39.35	2.29

Table A3 Current and THD_i at branch 5.

Case	Branch 5					
	Ph1		Ph2		Ph3	
Current	I (A)	THD_i (%)	I (A)	THD_i (%)	I (A)	THD_i (%)
I	45.22	0.00	44.13	0.00	43.75	0.00
II	61.07	0.92	62.04	0.92	64.55	0.90
III (T)	50.43	2.20	67.26	1.80	71.62	1.60
III (S)	49.43	1.93	68.94	1.52	72.19	1.36
III (F)	49.77	3.03	68.36	2.65	72.00	2.11
IV (T)	23.1	3.81	42.19	2.06	50.63	1.88
IV (S)	21.77	3.45	46.81	1.75	51.64	1.54
IV (F)	22.21	5.95	45.23	3.46	51.29	2.62

Table A4 Current and THD_i at branch 6.

Case	Branch 6					
	Ph1		Ph2		Ph3	
Current	I (A)	THD_i (%)	I (A)	THD_i (%)	I (A)	THD_i (%)
I	39.66	0.00	34.59	0.00	28.02	0.00
II	50.59	1.00	35.97	0.93	35.83	0.96
III (T)	44.00	2.42	39.02	1.60	38.29	1.90
III (S)	41.73	2.14	38.99	1.34	39.34	1.93
III (F)	42.49	3.48	39.06	1.78	38.98	2.53
IV (T)	10.44	7.12	28.06	1.8	25.54	2.09
IV (S)	7.13	9.64	27.87	1.33	26.83	1.73
IV (F)	8.23	15.15	27.93	1.97	26.39	3.20

Appendix B: Line and Consumer Data

Table B1 Load distribution by consumer.

Branch	Peak load			Single phase						3 Phase	
	P (kW)	Q (kVAr)	Consumers	P1	P2	P3	Q1	Q2	Q3	P	Q
1	1.9	0.76	4	0.95	0.48	0.48	0.38	0.19	0.19	--	--
	2.6	1.04	2	--	--	--	--	--	--	2.60	1.04
2	2.9	1.16	3	0.97	0.97	--	0.39	0.39	--	0.97	0.39
	18	7.2	14	6.43	6.43	5.14	2.57	2.57	2.06	--	--
	9.3	3.72	12	3.10	3.10	3.10	1.24	1.24	1.24	--	--
3	36.2	14.48	21	6.90	6.90	5.17	2.76	2.76	2.07	17.24	6.90
	15.1	6.04	11	5.49	4.12	4.12	2.20	1.65	1.65	1.37	0.55
	5.2	2.08	3	1.73	1.73	1.73	0.69	0.69	0.69	--	--
	0.4	0.16	1	0.40	--	--	0.16	--	--	--	--
	2.3	0.92	3	0.77	0.77	--	0.31	0.31	--	0.77	0.31
4	8.9	3.56	5	1.78	1.78	--	0.71	0.71	--	5.34	2.14
	17.9	7.16	8	4.48	2.24	2.24	1.79	0.90	0.90	8.95	3.58
	11.6	4.64	6	3.87	1.93	1.93	1.55	0.77	0.77	3.87	1.55
	5.6	2.24	3	1.87	1.87	--	0.75	0.75	--	1.87	0.75
	6.7	2.68	3	2.23	--	--	0.89	--	--	4.47	1.79
5	6.6	2.64	7	1.89	1.89	0.94	0.75	0.75	0.38	1.89	0.75
	4.2	1.68	10	1.26	1.26	1.26	0.50	0.50	0.50	0.42	0.17
	8.1	3.24	10	3.24	2.43	2.43	1.30	0.97	0.97	--	--
	0.4	0.16	1	0.40	--	--	0.16	--	--	--	--
6	9.6	3.84	8	2.40	1.20	1.20	0.96	0.48	0.48	4.80	1.92
	13.9	5.56	7	3.97	3.97	1.99	1.59	1.59	0.79	3.97	1.59
Total	187.4	74.96	142	54.11	43.05	31.73	21.64	17.22	12.69	58.51	23.40

Table B2 Power transformer data.

PT (power transformer)	
S (kVA)	400
U_{MV} (kV)	15
U_{LV} (V)	400
R transformer (Ω)	0.00378
X transformer (%)	6%

Table B3 Branch and line data.

Branch	Bus		Length (m)	Phase & neutral	
	From	To		R (Ω/km)	X (Ω/km)
1	5	29	40	0.496	477.5E-6
	5	74	180	0.857	477.5E-6
2	74	57	95	1.300	477.5E-6
	57	75	156	2.942	455.3E-6
	5	64	105	0.202	318.3E-6
3	64	27	250	1.025	358.7E-6
	27	71	108	2.191	386.4E-6
	27	73	33	2.463	392.4E-6
	5	14	20	0.393	318.3E-6
	14	23	141	0.438	387.5E-6
4	23	25	132	0.695	428.0E-6
	25	69	102	1.303	440.8E-6
	25	15	168	1.841	451.7E-6
	5	31	126	2.627	378.9E-6
	31	32	20	3.361	392.4E-6
5	31	33	134	2.534	433.1E-6
	33	37	128	2.454	389.6E-6
	33	55	78	2.473	370.2E-6
6	5	12	78	1.067	318.3E-6
	12	26	152	1.522	459.5E-6
	26	40	93	2.463	464.7E-6

As no data was available for line capacity (C); the same value as stated in Ref. [1] was used; $C = 0.6 \times 10^{-9}$ F/km.